Supplementary Material for: "Wavelength-insensitive snapshot Stokes polarimetric imaging based on cascaded metasurfaces"

Xuanguang Wu,[a] Kai Pan,[a] Xuanyu Wu,[a] Xinhao Fan,[a] Liang Zhou,[a] Chenyang Zhao,[b] Dandan Wen,[a] Sheng Liu,[a] Xuetao Gan,[a] Peng Li,[a,*] Jianlin Zhao[a]

[a]Northwestern Polytechnical University, School of Physical Science and Technology, Key Laboratory of light field manipulation and information acquisition, Ministry of Industry and Information Technology, and Shaanxi Key Laboratory of Optical Information Technology, No.1 Dongxiang Road, Chang'an District, Xi'an, China,710129
[b]Northwestern Polytechnical University, Analytical and Testing Center, No.1 Dongxiang Road, Chang'an District, Xi'an, China,710129

*****Peng Li**,** E-mail: pengli@nwpu.edu.cn

Note 1: Design of cascaded metasurfaces

The 2D polarization grating metasurface is located in the spatial spectrum plane of the imaging object, to perform 2D spin-dependent splitting of incident light field, of which the modulation effects on the left- (LCP, depicted as $|L_{\text{in}}\rangle$) and right-handed circular polarizations (RCP, depicted as $|R_{\text{in}}\rangle$) of incident light filed with arbitrary polarization are expressed as

$$\begin{aligned} J_2(x,y)\cdot|R_{\text{in}}\rangle &= \eta_2 E_{R\text{in}}\left\{\exp\left[\mathrm{i}k\tan\theta(x+y)\right]+\exp\left[\mathrm{i}k\tan\theta(-x+y)\right]\right\}|L\rangle \\ J_2(x,y)\cdot|L_{\text{in}}\rangle &= \eta_2 E_{L\text{in}}\left\{\exp\left[\mathrm{i}k\tan\theta(x-y)\right]+\exp\left[\mathrm{i}k\tan\theta(-x-y)\right]\right\}|R\rangle \end{aligned}, \tag{S1}$$

where, $J_2(x, y)$ is the Jones matrix of the 2D polarization grating, k is the wave number, and θ depicts the grating diffraction angle, $|R\rangle$ and $|L\rangle$ represent the RCP and LCP, $E_{R\text{in}}$ and $E_{L\text{in}}$ depict the complex amplitude of RCP and LCP components of incident light field, respectively; η_2 is the diffraction efficiency of the first order of 2D polarization grating.

According to the Fourier transform theory, these linear phase shifts induce spatially separations of two spin components along the diagonal and antidiagonal directions in the imaging plane that corresponds to the Fourier transform of diffraction or lens. At the imaging plane, four spin components are

$$\begin{aligned} |R_1\rangle &= \eta_2 E_{R\text{in}}(x+\Delta, y+\Delta)|R\rangle \\ |R_2\rangle &= \eta_2 E_{R\text{in}}(x-\Delta, y+\Delta)|R\rangle \\ |L_1\rangle &= \eta_2 E_{L\text{in}}(x-\Delta, y-\Delta)|L\rangle \\ |L_2\rangle &= \eta_2 E_{L\text{in}}(x+\Delta, y-\Delta)|L\rangle \end{aligned}, \tag{S2}$$

where $\Delta=f\tan\theta$ is the transverse displacement in the imaging plane, with f depicting the focal length of the Fourier transform lens in $4f$ system.

The 1D polarization grating is placed in the plane behind the 2D one with a distance of Δz, of which the Jones matrix is denoted as $J_1(x, y)$, thus the modulation on the LCP and RCP components of idler light directly transmitted from the 2D polarization grating (denoted as $|R_{\text{idler}}\rangle$ and $|L_{\text{idler}}\rangle$)are expressed as

$$\begin{aligned} J_1(x,y)\cdot\left|L_{\text{idler}}\right\rangle &= \eta_1 E_{L\text{idler}} \exp\left[\mathrm{i}k\tan\theta(x+y)\right]\left|R\right\rangle \\ J_1(x,y)\cdot\left|R_{\text{idler}}\right\rangle &= \eta_1 R_{R\text{idler}} \exp\left[-\mathrm{i}k\tan\theta(x+y)\right]\left|L\right\rangle \end{aligned}, \tag{S3}$$

where η_1 is the diffraction efficiency of the first order of 1D polarization grating. Considering the angular spectrum diffraction theory, it can be deduced that these two spin components at the same imaging plane can be described as

$$\begin{aligned} \left|R_3\right\rangle &= \eta_1 E_{R\text{idler}}(x-\Delta, y-\Delta)\exp\left[-\mathrm{i}2\pi\Delta z\tan\theta(x+y)/\lambda f\right]\left|R\right\rangle \\ \left|L_3\right\rangle &= \eta_1 E_{L\text{idler}}(x+\Delta, y+\Delta)\exp\left[\mathrm{i}2\pi\Delta z\tan\theta(x+y)/\lambda f\right]\left|L\right\rangle \end{aligned}, \tag{S4}$$

From Eq. S4, it can be seen that these spin components $|R_3\rangle$, $|L_3\rangle$ and orthogonal spin components $|L_1\rangle$, $|R_1\rangle$ overlap at the same dislocations in the diagonal direction. The longitudinal displacement of 1D polarization grating generate linear phase shifts on the outgoing spin components with respective to those diffracted from the 2D one. These phase shifts are conjugate and proportional to the grating diffraction angle θ and the longitudinal displacement Δz, which provide degrees of freedom to control the interferometric images and phase measurement accuracy.

Note 2: Design of 1D polarization grating

The angular spectrum diffraction theory is used to calculate the modulation effect of the 1D polarization grating on the light field. Assuming that the light field in the initial plane of a 4*f* optical imaging system is $E_{\text{in}}(x_0, y_0)$, the spatial spectrum $E_1(f_x, f_y)$ thus can be expressed as

$$E_1(f_x, f_y) = F\left\{E_{\text{in}}(x_0, y_0)\right\}, \tag{S5}$$

where f_x=-$x_1/\lambda f$ and f_y=-$y_1/\lambda f$. The light field distribution $E_2(x_2, y_2)$ at the plane behind the spectrum plane with an interval of Δz can be obtained as

$$\begin{aligned} E_2(x_2, y_2) &= F^{-}\left\{F\left\{E_1(f_x, f_y)\right\}\exp\left[-\mathrm{i}\pi\lambda\Delta z\left(f_x^2+f_y^2\right)\right]\right\} \\ &= F^{-}\left\{E_{\text{in}}(-\lambda f f_x, -\lambda f f_y)\exp\left[-\mathrm{i}\pi\lambda\Delta z\left(f_x^2+f_y^2\right)\right]\right\} \end{aligned}. \tag{S6}$$

Here we only take the phase modulation of RCP component as an example, and the phase modulation of the 1D polarization grating is $\exp(\mathrm{i}kx\tan\theta)$, where k is wave number.

On the modulation of 1D polarization grating, the output light field $E'_2(x_2, y_2)$ is

$$
\begin{aligned}
E_2^{'}(x_2, y_2) &= E_2(x_2, y_2)\exp(\mathrm{i}kx\tan\theta) \\
E_2^{'}(x_2, y_2) &= F^{-1}\left\{\left(E_{\mathrm{in}}(-\lambda f f_x, -\lambda f f_y)\exp\left[-\mathrm{i}\pi\lambda\Delta z\left(f_x^2 + f_y^2\right)\right]\right) * F\left\{\exp(\mathrm{i}kx\tan\theta)\right\}\right\} \\
&= F^{-1}\left\{E_{\mathrm{in}}(-\lambda f f_x + f\tan\theta, -\lambda f f_y)\exp\left[-\mathrm{i}\pi\lambda\Delta z\left(\left(f_x - \frac{\tan\theta}{\lambda}\right)^2 + f_y^2\right)\right]\right\}.
\end{aligned}
\tag{S7}
$$

Considering the reverse propagation of this light field along the -*z* direction, to the light field E_{2f} (x_2, y_2) at the spectrum plane of the 4*f* optical system thus can be expressed as

$$
\begin{aligned}
E_{2f}(f_x, f_y) &= F^{-1}\left\{F\left[E_2^{'}(x_2, y_2)\right]\exp\left[\mathrm{i}\pi\lambda\Delta z\left(f_x^2 + f_y^2\right)\right]\right\} \\
&= F^{-1}\left\{E_{\mathrm{in}}(-\lambda f f_x + f\tan\theta, -\lambda f f_y)\exp\left[\mathrm{i}\pi\lambda\Delta z\left(2f_x\frac{\tan\theta}{\lambda} - \left(\frac{\tan\theta}{\lambda}\right)^2\right)\right]\right\}.
\end{aligned}
\tag{S8}
$$

Consequently, the output light field $E_{\mathrm{out}}(x_3, y_3)$ can be obtained

$$
\begin{aligned}
E_{\mathrm{out}}(x_3, y_3) &= F\left\{E_{2f}(x_2, y_2)\right\} \\
&= \exp\left(-\mathrm{i}\pi\lambda\Delta z\left(\frac{\tan\theta}{\lambda}\right)^2\right)E_{\mathrm{in}}(-x_3 + f\tan\theta, -y_3)\exp\left[\mathrm{i}2\pi\Delta z\frac{\tan\theta}{\lambda f}x_3\right].
\end{aligned}
\tag{S9}
$$

The first term of the output light field is constant, thus Eq. (S4) is obtained. Here, the phase modulation of polarization grating is selected as exp (i*kx*tanθ) with $k=2\pi/\lambda$. Considering the diffraction dispersion of the polarization grating, the mechanism by which the longitudinal displacement of the polarization grating near the spectral plane of the 4*f* optical system at different wavelengths controls the outgoing light field can be derived, as shown in Eq. S10.

$$
E_{\mathrm{out}}(x, y) = \exp\left(\mathrm{i}\pi\lambda\Delta z\left(\frac{\tan\theta_0}{\lambda_0}\right)^2\right)E_{\mathrm{in}}\left(-x + \frac{\lambda}{\lambda_0}f\tan\theta_0, y\right)\exp\left(-\mathrm{i}2\pi\Delta z\frac{\tan\theta_0}{\lambda_0 f}x\right). \tag{S10}
$$

Where λ_0 is the design wavelength of the polarization grating, λ is the incident wavelength, and θ_0 is the diffraction angle of the grating at the theoretical design wavelength. It can be further deduced that, when the polarization grating period is constant, changing the wavelength of the incident light only induces the linear displacement in the imaging plane, as $\Delta x=\lambda/\lambda_0 * f\tan\theta_0$, and does not change the magnitude of the linear phase shift.

Note 3: Resolution of imaging systems

Here we only discuss the imaging resolution limitations introduced by metasurface and 4*f* optical imaging system, without considering microscopy imaging systems. The two-dimensional (2D) polarization grating is located in the spectrum plane of the 4*f* optical system, and its radius size *r* limits the resolution of the 4*f* optical imaging system, that is, $f_I = r/(\lambda f)$. On the other hand, the

imaging resolution of the system also depends on the interferograms period. After fully considering the influence of the zero-order component of the interferograms in its spectrum plane, the spatial frequency shift amount corresponding to the linear phase shift introduced by the 1D polarization grating is $f_a=(\Delta z\tan\theta)/(\lambda f)$, and the theoretical imaging resolution is $f_{\Delta\varphi}=f_a/3$. When the wavelength and lens focal length are given, the magnitude of the linear phase shift is only related to the diffraction angle θ and the displacement Δz. The diffraction angle also determines the size of the field of view (FoV). Theoretically, 1D polarization grating needs to completely cover the diffraction light field of zero-order light without affecting the higher-order diffraction light field. Therefore, the size of Δz needs to be carefully selected, which affects the range of action of the 1D polarization grating on the zero-order diffraction light field, and ultimately affects the imaging resolution and FoV size.

We have provided a detailed characterization of the imaging resolution of the experimental system. Firstly, based on experimental parameters such as the lens focal length f=7.5 cm and the radius r=1.25 mm of the 2D polarization grating, the coherent transfer function (CTF) of the imaging system under a 633 nm light source can be calculated, which the cutoff frequency is $f_{CTF}\approx$26.34 lp/mm. And the actual imaging resolution of the system was characterized by coherent imaging of 1951 USAF Target (THORLABS, R1DS1N), and the results are shown in Fig S1(a). The system can distinguish the minimum line pair of Group 4 Element 5, which corresponds to 25.39 lp/mm, a result that is consistent with theoretical calculations. In order to further quantitatively characterize the imaging resolution limit of the system, the point spread functions (PSFs) of the LCP and RCP components were experimentally measured, and the corresponding modulation transfer functions (MTFs) were calculated, as shown in Fig S1(b). According to 2D distributions of the MTFs, the LCP and RCP components exhibit good imaging resolution in both radial and angular directions. From the MTF curves in Fig. S1(c), it can be seen that the cutoff frequency for incoherent imaging is approximately $f_{MTF}\approx$52 lp/mm. This confirms the theoretical relationship where f_{MTF} is twice the f_{CTF}, further characterizing the imaging resolution of the measurement system and aligning with the theoretical design.

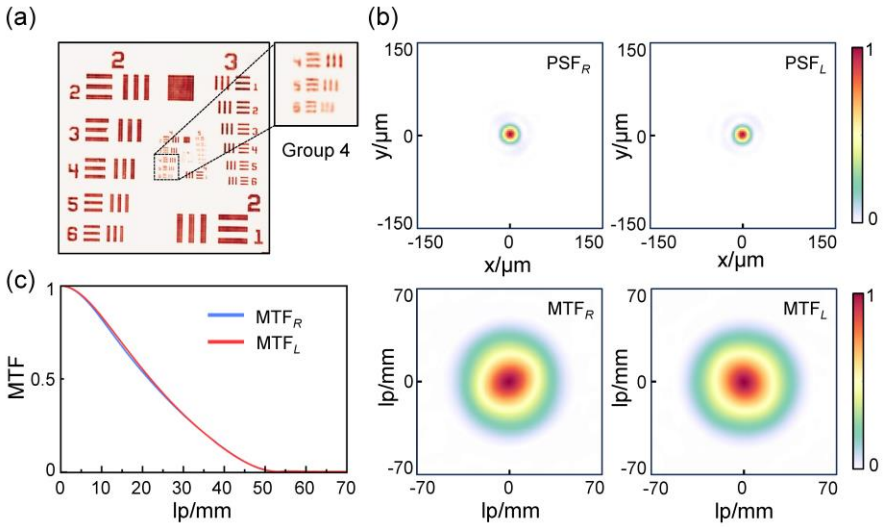

Fig. S1 Resolution characterization of system. (a) 1951 USAF Target (THORLABS, R1DS1N) imaging resolution test. The inset is an enlarged view of Group 4 Element 4-6, with line widths of 22.62 lp/mm, 25.39 lp/mm, and 28.50 lp/mm, respectively. (b) Measured distributions of PSFs and MTFs of the RCP and LCP light. (c) The MTFs of the imaging system show that the cutoff frequencies of the LCP and RCP light are approximately 52 lp/mm.

Note 4: Theoretical analysis of rectangular phase grating

The phase distribution of the rectangular phase grating is t, wherein the grating period is d (d=a+b), with a and b depicting the widths of binary (0 and π) phase distributions, the distribution of t thus can be expressed as

$$t(x)=\sum_m\left\{\delta(x-md)*\mathrm{rect}\left(\frac{x}{a}\right)+\delta(x+d/2-md)*\mathrm{rect}\left(\frac{x}{b}\right)\exp(\mathrm{i}\pi)\right\}. \tag{S10}$$

The far-field diffraction order of this rectangular phase grating can be expressed by the Fourier transform as

$$\begin{aligned} F\{t(x)\} &= \sum_m\left\{\left[a\,\mathrm{sinc}(af_x)+b\,\mathrm{sinc}(bf_x)\exp(\mathrm{i}2\pi f_x d/2)\exp(\mathrm{i}\pi)\right]\exp(-\mathrm{i}2\pi f_x md)\right\} \\ &= \sum_m\left\{\left[a\,\mathrm{sinc}(m\frac{a}{d})+b\,\mathrm{sinc}(m\frac{b}{d})\exp(\mathrm{i}m\pi)\exp(\mathrm{i}\pi)\right]\exp(-\mathrm{i}2\pi f_x md)\right\} \\ f_x &= \frac{\sin\theta}{\lambda}=\frac{m}{d} \end{aligned}. \tag{S11}$$

The intensity of the m-order diffraction order is given by

$$\begin{aligned} I_m &= \left|a\,\mathrm{sinc}(m\frac{a}{d})+b\,\mathrm{sinc}(m\frac{b}{d})\exp(\mathrm{i}m\pi)\exp(\mathrm{i}\pi)\right|^2 \\ &= \frac{4\sin^2(am\pi/d)}{(m\pi)^2} \end{aligned}. \tag{S12}$$

When a=0.5d, the theoretical intensity of the zeroth order component is 0%, and the intensity of the first order component reaches its maximum value of 40.53%, i.e., $\eta_2=\sqrt{2}/2*\sin(\delta/2)*\sqrt{0.4053} \approx 38\%$.

Note 5: Image registration

Considering the translation invariance of grating, this cascaded metasurfaces interferometer needs no registration and mechanical moving parts. To accurately reconstruct the Stokes parameter distributions, the amplitude images (obtained from I_R and I_L directly transmitted by the 2D grating) and phase retardation image (obtained by digital holography from the interferograms) require once registration, here we use the checkerboard calibration method for image registration.

Because the 1D polarization grating does not introduce additional image displacement, we only consider the registration of four first-order images of the 2D grating. During the image registration process, we select a checkerboard as object, of which the output images recorded by CMOS is shown in Fig. S2, and then perform corner point detection on these images. Using one of these images as the benchmark, the affine transformation matrices of other three images thus can be calculated, and then images alignment perform. In subsequent measurements, the existing affine transformation matrix can be directly used to match and align recorded images.

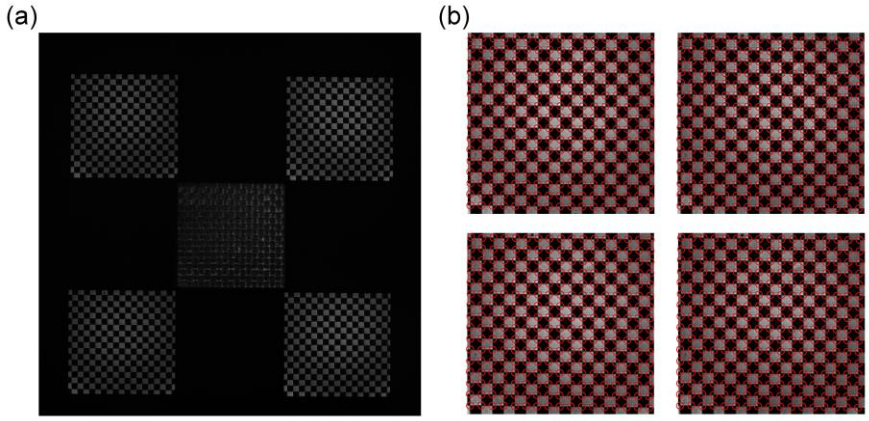

Fig. S2 Schematic illustration of checkerboard image registration. (a) Recorded checkerboard image. (b) Sub-image corner recognition.

Note 6: Feasibility verification

We compared the measured Stokes vector distributions by cascaded metasurfaces interferometer and traditional intensity method. Fig. S3, S4, and S5 display the Stokes vector distributions of the

horizontally polarized beam after passing through the first- and second-order vortex waveplates, and the liquid crystal depolarizer, respectively. The measurement results of two methods are consistent, verifying the feasibility of this method for polarization measurement.

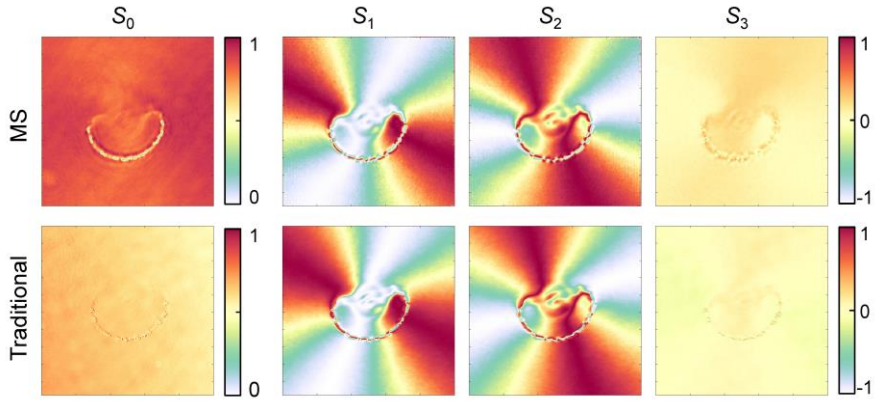

Fig. S3 Experimental results of the first-order vortex waveplate. Upper: cascaded metasurfaces interferometer; lower: traditional intensity measurement method.

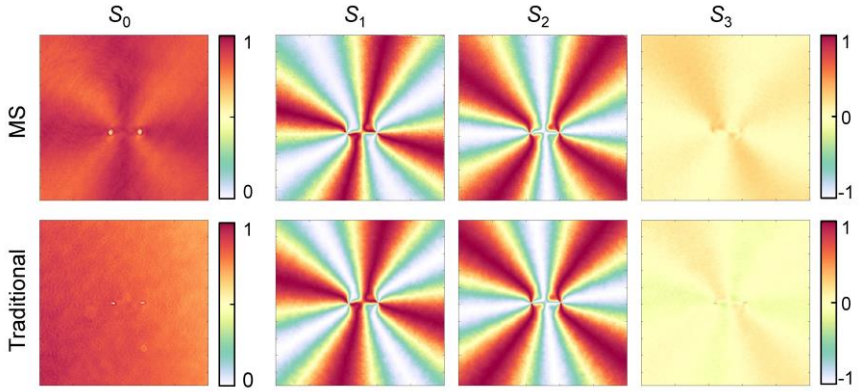

Fig. S4 Experimental results of second-order vortex waveplate. Upper: cascaded metasurfaces interferometer; lower: traditional intensity measurement method.

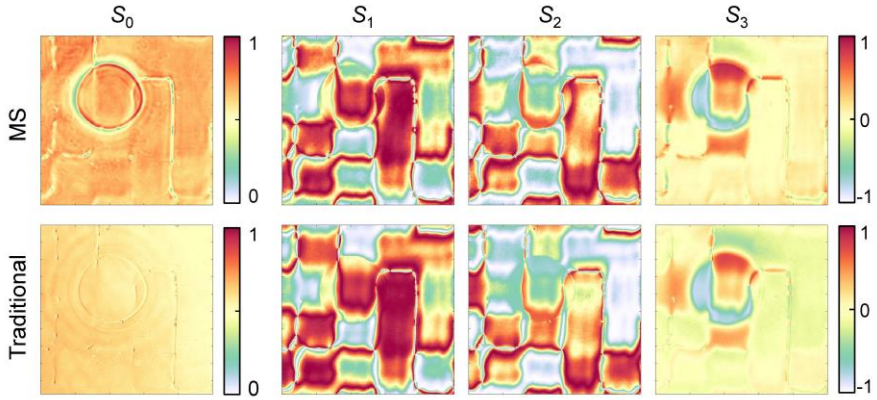

Fig. S5 Experimental results of the liquid crystal depolarizer. Upper: cascaded metasurfaces interferometer; lower: traditional intensity measurement method.

Note 7: Birefringence effect of liquid crystal molecules

The liquid crystal (LC) molecule can be regarded as a uniaxial crystal. On the planes parallel to the optical axis of the LC molecule and perpendicular to the optical axis, the dielectric constants are $\varepsilon_{//}$ and $\varepsilon_{\perp}$, respectively, and the refractive index shown is n_e (extraordinary light refraction index) and n_o (ordinary light refractive index). Fig. S6(b) shows the refractive index ellipsoid model of a single LC molecule. The angle between the optical axis of the LC molecule (i.e., the liquid crystal molecule director ***n***) and the incident light wave vector direction ***k*** is defined as γ. The rotation angle of the LC molecule director ***n*** in the vertical wave vector ***k*** plane is θ (θ is also called the orientation angle of the liquid crystal molecules). The light filed is incident perpendicularly to the LC cell substrate. When the orientation angle is zero, the projection direction of the LC molecule director ***n*** on the substrate is the *x*-axis, and the wave vector direction ***k*** of the incident light is the *z*-axis. When no external voltage is applied, the director ***n*** is perpendicular to the wave vector ***k***, this is $\gamma=\pi/2$, and the cross-section of the refractive index ellipsoid corresponding to the orthogonal components of the incident light is an ellipse, with the long axis n_e and the short axis n_o, birefringence index $\Delta n=n_e-n_o$.

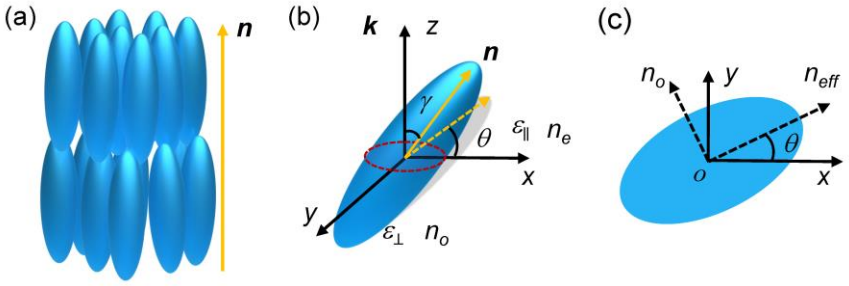

Fig. S6 Birefringence theory of LC molecules. (a) The director of the LC molecules n; (b) Under a certain voltage U and orientation angle θ, the refractive index ellipsoid of the LC molecules; (c) The refractive index ellipse of the plane where the two orthogonal components of the incident light wave are located.

When a voltage *U* is applied to both ends of the LC device, causing an electric field with an electric field strength ***E*** to be generated between the upper and lower substrates, based on the dielectric anisotropy of the LC, the external electric field will produce forces in opposite directions on both ends of the LC molecules. The director ***n*** of the LC molecules is driven to rotate in the direction of the electric field ***E***, that is, γ changes with the voltage *U*. When the orientation angle

of the LC molecules is zero, the major axis of the cross-sectional ellipse corresponding to the two orthogonal components of the incident light is n_{eff} and the minor axis is n_o, and $n_{eff}(\gamma)=n_o \cdot n_e/\sqrt{(n_o^2\sin^2\gamma+n_e^2\cos^2\gamma)}$. At this time, birefringence index $\Delta n=n_{eff}(\gamma)-n_o$. When the incident light with wavelength λ passes through a LC device with thickness d, the accumulated optical path of ordinary light and extraordinary light is different, and its propagation phase retardation is $\delta=2\pi\Delta nd/\lambda=2\pi(n_{eff}(\gamma)-n_o)d/\lambda=\varphi_e-\varphi_o$, which changes with applied voltage. When the orientation angle θ of the LC molecules changes, the azimuthal angle of the refractive index ellipse in Fig. S6(c) also rotates accordingly.

The optical wavefront control of the LC geometric phase device is mainly determined by the amplitude transmittance T_e and T_o of the long and short axes of the LC molecules, the phase retardation δ and the orientation angle θ. Its wavefront modulation effect can be expressed by the Jones matrix as

$$J_M(\theta)=R(-\theta)\begin{bmatrix} T_e e^{i\varphi_e} & 0 \\ 0 & T_o e^{i\varphi_o} \end{bmatrix} R(\theta), R(\theta)=\begin{bmatrix} \cos\theta & -\sin\theta \\ \sin\theta & \cos\theta \end{bmatrix}. \tag{S13}$$

φ_e and φ_o are the phase retardation of the long and short axes, and $R(\theta)$ is the rotation matrix. In general, $T_e=T_o=T_0$. After substituting into Jones matrix, we can get

$$J_M(\theta)=T_0 e^{i\frac{\varphi_e+\varphi_o}{2}}\begin{bmatrix} \cos\frac{\delta}{2}+i\sin\frac{\delta}{2}\cos 2\theta & -i\sin\frac{\delta}{2}\sin 2\theta \\ -i\sin\frac{\delta}{2}\sin 2\theta & \cos\frac{\delta}{2}-i\sin\frac{\delta}{2}\cos 2\theta \end{bmatrix}. \tag{S14}$$

When a circularly polarized light $[1, \pm i]^T$ is incident, the output light field is

$$\mathbf{E}_{out}=T_0\exp\left(i\frac{\varphi_e+\varphi_o}{2}\right)\left\{\cos\frac{\delta}{2}\begin{bmatrix}1\\ \pm i\end{bmatrix}+\sin\frac{\delta}{2}\exp\left(\pm i2\theta+i\frac{\pi}{2}\right)\begin{bmatrix}1\\ \mp i\end{bmatrix}\right\}. \tag{S15}$$

It can be seen from the Eq. S15 that by manipulating the orientation angle θ of the LC molecules, the geometric phase of the outgoing light field can be controlled, and the modulation efficiency of the geometric phase can be controlled by phase retardation δ. When the phase retardation $\delta=\pi$, the co-polarization component is zero, and the modulation efficiency is maximum.

The orientation angle distribution of LC molecules in the LC polarizing grating is $\theta=\text{angle}(kx\tan\phi)/2$. Under the operating voltage of $\delta=\pi$, the modulation phases of LCP and RCP components are $\pm kx\tan\phi$, respectively, with $\phi=0.015$ rad. The phase retardation between the LCP and RCP is $2kx\tan\phi$. Under operating voltage of $\delta\neq\pi$, due to the influence of the co-polarized polarization component, the phase retardation between LCP and RCP does not satisfy this

theoretical relationship. Therefore, by measuring the phase retardation between LCP and RCP and comparing it with the theoretical value, the operating voltage of the LC polarizing grating can be obtained. Through experimental measurements, the LC polarizing grating has high modulation efficiency at a voltage of 2.0-4.0V.

Note 8: Experimental setup of partially coherent light illumination

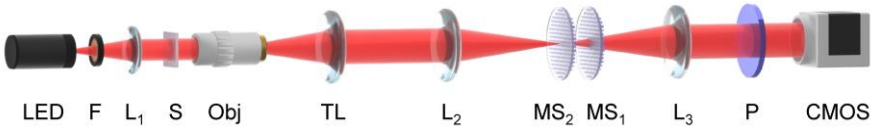

Fig. S7 Experimental setup of partially coherent light illumination.

The experimental setup of partially coherent light illumination is shown in Fig. S7, wherein F is the filter (GCC-202208). L1 is the collimating lens of the LED, with a focal length of 5 cm, and S is the sample to be tested. Obj is a microscope objective with the magnification of 10X, and TL is a tube lens. The focal length of L2 and L3 is 7.5 cm, together forming a 4*f* optical system. MS_2 and MS_1 are 2D and 1D polarization gratings, respectively, with P as the polarizer and COMS (Hamamatsu C11440-42U40) as the optical sensor, used for image acquisition.

We further explored the impact of LED light source at other wavelengths with different full width at half maxima (FWHM), including 623 nm (FWHM=14.4 nm), 626 nm (FWHM=9.2 nm), and 520 nm (FWHM=31.8 nm). Firstly, experiments were conducted on the second-order LC vortex waveplate using light sources with different bandwidths of FWHM=14.4 nm and FWHM=9.2 nm, of which the central peaks are located at 623 nm and 626 nm (because the central wavelengths of the filter are different), and the results are shown in Fig. S8(a). The measured results include the Stokes parameters and the phase retardation $\Delta\varphi$ between the left- and right-handed circular polarization components. It can be seen that the S_0 and S_3 components of different bandwidths are essentially consistent. However, the S_1 and S_2 components are affected by the phase retardation $\Delta\varphi$ and differ, mainly due to the inaccuracy in solving the phase retardation of a broader bandwidth of light source. Further analysis shows that the bandwidth of the light source directly affects the contrast of the interference fringes, thereby affecting the accuracy of digital holographic interferometry measurements. The contrast analysis of the interferograms under illuminations of light sources at 623 nm (FWHM=14.4 nm) and 626 nm (FWHM=9.2 nm), as shown in Figs. S8(b-d). Figures S8(b) and S8(c) are the interferograms in the cases of 14.4 nm and 9.2 nm bandwidths,

respectively. Figure S8(d) presents the contrast of interference fringes in these two cases. Clearly, the light source with a narrower bandwidth has a higher contrast, which allows for more precise interference measurements.

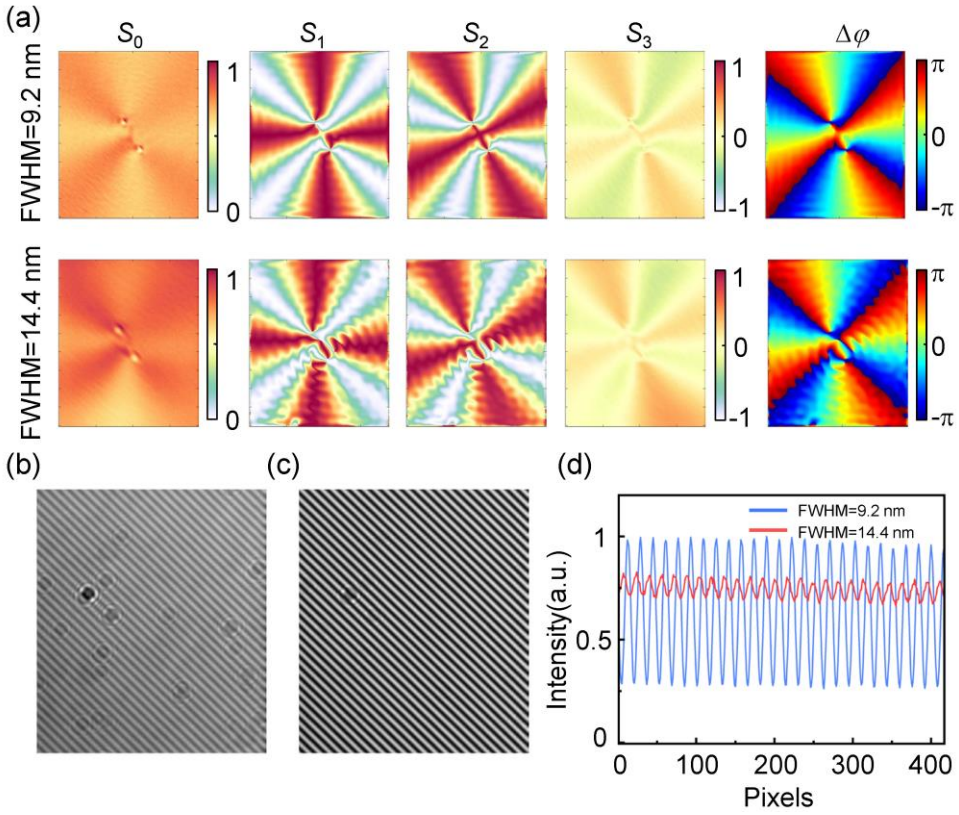

Fig. S8 Comparative analysis of experimental results for LED light sources with different FWHM. (a) The results of Stokes parameters and phase retardation $\Delta\varphi$ for the second-order LC vortex waveplate with different FWHM=9.2 nm(upper) and 14.4 nm(lower), respectively; (b) Interferogram of light with FWHM=14.4 nm; (c) Interferogram of light with FWHM=9.2 nm; (d) Interference fringes contrast analysis.

This polarimetric imaging methods uses tilted phases to spatially multiplex orthogonal polarization components, it can produce diffraction dispersion. When the incident light source has a broad bandwidth, it affects the imaging quality. Figure S9 shows the observed results of polarimetric imaging using only the two-dimensional polarization grating, with the incident light source having a central wavelength of 520 nm and 31.8 nm bandwidth. As shown in Fig. S9(a), the two-dimensional polarization grating can still achieve effective diffraction separation of two circularly polarized components under broadband light incidence. However, due to the diffraction dispersion introduced by the broadband light source, the checkerboard pattern used for alignment and standardization in Fig. S9(b) has been severely distorted along the diffraction angle direction,

making it is impossible to achieve clear imaging. Thereby the bandwidth of this polarimetric imaging system is about 14 nm.

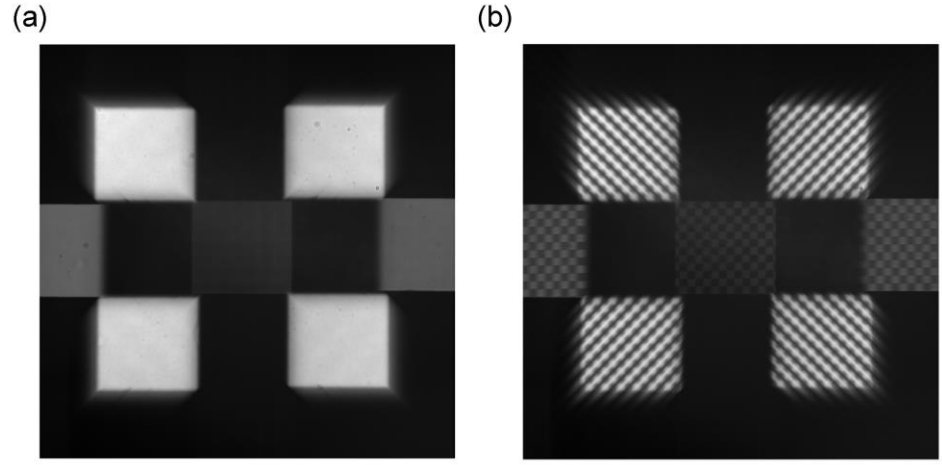

Fig. S9 Imaging dispersion analysis of two-dimensional polarization gratings under the illumination of broadband light sources with FWHM=31.8 nm. (a) Imaging of square hole illuminated by linearly polarized planar light; (b) Imaging of a checkerboard pattern.